Surface & Coatings Technology 397 (2020) 126016

Contents lists available at ScienceDirect

Surface & Coatings Technology

journal homepage: www.elsevier.com/locate/surfcoat

PEO-Chameleon as a potential protective coating on cast aluminum alloys for high-temperature applications

Asghar Shirani[a], Tasha Joy[a], Aleksey Rogov[b], Mengyu Lin[b], Aleksey Yerokhin[b], Jon-Erik Mogonye[c], Andras Korenyi-Both[d], Samir M. Aouadi[a], Andrey A. Voevodin[a,*], Diana Berman[a,*]

[a] Department of Materials Science & Engineering, University of North Texas, TX, United States
[b] University of Manchester, Manchester, United Kingdom
[c] U.S. CCDC Army Research Laboratory, Adelphi, MD, United States
[d] Tribologix INC., Golden, CO, United States

ARTICLE INFO

Keywords:
High-temperature coating
Chameleon
Friction
Wear
Plasma electrolytic oxidation

ABSTRACT

Hybrid dual-phase coatings composed of an A356 aluminum alloy modified by plasma electrolytic oxidation (PEO) and burnished with graphite-MoS_2-Sb_2O_3 chameleon solid lubricant powders have been produced. The PEO layer provides high hardness and load support while the solid lubricant powders reduce friction. These hybrid coatings were tribotested against steel and silicon nitride counterparts in air from 25 °C to 300 °C and using variable contact loads. The open porosity and surface roughness of the PEO layers were reduced considerably by the burnishing process. Polishing of the PEO surfaces prior to burnishing significantly reduced the resulting coefficient of friction (COF) of the hybrid coating. In-situ Raman spectroscopy revealed the chemical stability of the dual phase coatings at temperatures up to 300 °C with no signs of oxidation or reduction of the chameleon components. COF values ranged from 0.2 at room temperature down to 0.02 at 300 °C. The observed low friction values were attributed to the synergism between PEO and chameleon layers that promote defect healing and adaptive behavior of the coating. Top view scanning electron microscopy (SEM) and cross-sectional transmission electron microscopy (TEM) confirmed that the thermo-mechanical stimulus caused the chameleon coating to fill the voids in the PEO layer. In-situ Raman spectroscopy revealed that the lubricating phases, i.e. MoS_2 and graphite, were protected from oxidation by the porous PEO structure. These lubricious phases formed a transfer film in the wear tracks and the counterpart bodies as a result of the contact pressure (up to 1.4 GPa) and thermal energy, which led to an order of magnitude reduction in the COF at high temperatures. The low shear strength of MoS_2 and graphite and the good adhesion and integration of the chameleon coating with the PEO sublayer due to high contact pressures during sliding were responsible for the ultra-low friction behavior of the composite coating.

1. Introduction

The increased need for light-weight, high-strength, corrosion-resistant materials for energy-efficient vehicles in the aerospace and automotive industries has led to many recent studies on advancing aluminum, titanium, and magnesium-based alloys for such applications. One major drawback of using light-weight alloys in mechanical systems is their poor tribological behavior [1] that results in high friction and wear characteristics. Cast Al alloys are widely used as materials for manufacturing engine blocks. To protect Al from the heat and wear, the combustion cylinders of reciprocating engines frequently use steel inserts or liners; however, recently more and more automotive engines use thermally-sprayed coatings on the cylinder bore [2].

Considerable efforts have been dedicated to improving the tribological performance of Al components by modifying their surface structure and composition. Such surface modification approaches include anodizing [3,4], laser-based surface texturing [5,6], and the application of various coatings by physical [7,8] or chemical [9] vapor deposition methods. The use of lubricants is a potentially viable option to enhance the tribological properties of Al-based materials. While liquid lubricants are efficient to reduce friction and wear in metallic surfaces [10,11] [12], normally these are limited to operating temperatures < 200 °C. At

* Corresponding authors.
E-mail addresses: Andrey.Voevodin@unt.edu (A.A. Voevodin), Diana.Berman@unt.edu (D. Berman).

https://doi.org/10.1016/j.surfcoat.2020.126016
Received 29 April 2020; Received in revised form 1 June 2020; Accepted 2 June 2020
Available online 05 June 2020
0257-8972/ © 2020 Elsevier B.V. All rights reserved.

higher temperatures, oxidation and the chemical evolution of material surfaces during sliding lead to the loss of liquid lubrication and the eventual failure of moving components [13,14]. For temperatures > 200 °C, the use of solid lubricants and elimination of liquid lubricants are usually the best choice [15–17]. Soft metals such as lead, gold, or silver were reported to provide shear accommodation during sliding from 200 to about 500 °C [18]. Alternatively, metal oxide coatings with a lamellar crystal structure with weak inter-planar cohesive bonds can be applied for easier shearing but are usually most effective at $T > 500$ °C [19]. Recently, adaptive coatings [20,21], including self-healing materials [22], were demonstrated to be lubricious over a wide range of temperatures facilitated by thermo-mechanical stimuli that activate the desired lubricant at the surface. The main challenge that remains is the lack of understanding whether these coating materials are suitable for light-weight alloys; i.e., whether they work reliably over a wide range of temperatures, environments, and load conditions similar to those experienced in their potential automotive or aerospace engine applications.

Chameleon coatings were reported to provide optimal performance in variable temperature and humidity conditions [23]. These coatings usually consist of a combination of solid lubricants, such as MoS_2 that reduce friction in the absence of water vapors [24] or when the basal plane anisotropy long-range order is provided [25], graphite that is functional at low temperature and in the presence of humidity [26], and boron nitride that tribologically is more effective for high-temperature needs [27]. The environment triggers the appropriate lubricant to be released to the surface of the chameleon coating. Changes in the environment include a controlled ambient temperature [28], the absence of moisture [29,30], or a range of temperatures [31] [32].

The major limitation of chameleon coatings is being soft which reduces their wear protective effect on Al alloy surfaces [33]. To overcome such a potential drawback, a promising solution is a modification of the surface of the aluminum alloy material to form a hard wear protective oxide layer and to embed the chameleon coating material inside this layer. The cast aluminum alloy substrate surface can be successfully transformed into hard alumina-based layers of an order of a few 100-micrometer thickness range using the plasma electrolytic oxidation (PEO) approach [34]. PEO coatings are usually grown anodically, in silicate alkaline electrolytes, above breakdown voltage of the formed oxide layer. This results in plasma-assisted electrochemical conversion of the Al alloy surface, which provides metallurgical bonding to the metal substrate leading to surface structures comprising a dense and hard alumina inner layer which gradually transitions to a softer and more porous Al-Si-O surface layer. The application of PEO coatings on wrought Al alloys was shown to provide considerably extended abrasion and adhesive wear resistance for such treated surfaces [35,36]. Variations in processing parameters allow controlling surface porosity and roughness, as well as the overall thickness of PEO coatings [37]. However, for cast Al—Si alloy substrates, the major problem is presented by a coarse heterogeneous structure of the alloy containing Al—Si eutectic which is preferentially oxidized, leading to the formation of a non-uniform porous surface structure with inferior mechanical and tribological properties [38–40]. Specifically, anodic oxidation of Al is hindered by the formation of the anodic alumina layer, whereas oxidation of Si in the eutectic phase yields soluble silicate anions and the grains will remain electrochemically active until either all Si in it is consumed or a solubility limit of silicate ions in the electrolyte is reached and they would start precipitating back to the surface [38–40]. Attempts have been made to resolve this problem by refining alloy microstructure [41], modifying electrolyte composition [42,43], and/or applying sequential treatments in different electrolytes [44]. Since these approaches often led to more complex and laborious manufacturing routes, or coatings with insufficient thickness and mechanical properties to be used in structural applications, the studies of PEO coating tribology on cast Al alloys are rather scarce and those concerned with high-temperature tribology are virtually non-existent.

Despite that, surface morphology and residual porosity of PEO coatings generally provide ideal conditions for adherence of solid lubricant chameleon compositions, creating reservoirs of adaptive solid lubricant in hard wear-resistant and relatively thick protective oxide layers. A chameleon coating composition based on graphite, MoS_2, and Sb_2O_3 mixture [45] can be applied to the surface of the PEO coatings by a simple, low-cost burnishing process. Such a PEO-Chameleon coating combination was demonstrated by recent fretting wear studies to maintain the lubricity and to extend the lifetime of the coating on a rough AA6082 Al alloy substrate [33,39]. These studies were focused on testing the PEO-Chameleon coatings over a range of humidity conditions against steel and ceramic counterparts at room temperatures.

In the current study, we expand this approach to cast Al alloy substrates to further evaluate the tribological potential of PEO-Chameleon coatings upon their exposure to high-temperature conditions. We use in-situ Raman analysis [46] and SEM to evaluate the origin of high-temperature lubricity up to 300 °C. Our results indicate that the roughness of the PEO matrix is important in defining the wear resistance of the coating. At high temperatures, shear-assisted healing of microcracks allows the reduction in friction and wear and provides good thermal stability. We show that the PEO matrix also provides good thermal barrier characteristics essential for engine applications which protect the underlying aluminum substrate from exposure to heat and prevent the reduction of yield strength at elevated temperature of the material.

2. Experimental

2.1. Coating

PEO-Chameleon coating was produced on an aluminum A356 substrate (Table S1), frequently selected for high-temperature automotive applications. The alloy was machined in 50 × 50 mm^2 coupons and hardened using the T6 heat treatment, which is an artificial aging treatment procedure. The PEO coatings were grown using the equipment described elsewhere [47]; a pulsed bipolar current waveform was applied at 1 kHz frequency, with anodic and cathodic current densities set at 100 and 130 mA/cm^2, respectively. The treatments were carried out for 65 min in an aqueous alkaline electrolyte containing 4 g/l KOH and 12 g/l Na_2SiO_3, at temperature 47 ± 2 °C. The as-deposited coatings with a thickness of 130–160 μm and surface roughness Ra = 50.1 ± 7.1 μm were subjected to two polishing cycles with SiC paper to achieve different combinations of residual thickness and surface roughness/open porosity (Table 1). Subsequently, a 5–8 μm top layer of a chameleon coating composition (graphite, MoS_2, and Sb_2O_3 with 2:2:1 wt. ratio) was burnished over the PEO by using a lint free

Table 1
PEO coating growth time, thickness, roughness before and after burnishing chameleon coating, and thermal conductivity of the samples.

Sample	Surface	PEO Coating thickness (μm)	Roughness before burnishing Ra (μm)	Roughness after burnishing Ra (μm)	Thermal conductivity (W/m K)
Al0	N.A	N.A	0.02 ± 0.005	N.A.	157.6 ± 13.3
Al1	As deposited	180–200	50.1 ± 7.1	43.9 ± 24.4	38.5 ± 1.7
Al2	Coarse polished	130–160	36.8 ± 3.0	19.1 ± 7.3	34.5 ± 2.1
Al3	Fine polished	28–32	3.4 ± 0.2	0.3 ± 0.05	36.7 ± 3.2

cloth with the Chameleon powder on it under the hand pressure as described in details in our previous work [45]. Uncoated aluminum coupons (Al0 in Table 1) were used for baseline comparisons. The error bars for the measurements are calculated from the standard deviation.

2.2. Tribology

The initial tribological assessment of the samples was performed using a home-built in-situ Raman pin-on-disk apparatus (Fig. 3a) with high-temperature capability. For in-situ Raman spectroscopy, a Renishaw Raman Microscope with green laser 532 nm wavelength was paired to a custom arrangement that allowed probing of the wear track on coated sample surfaces during sliding in high-temperature experiments as described earlier in detail [46]. The counterpart pins were 5 mm diameter, 5 mm length cylinders made of 52100 steel with initial roughness ~20 nm Ra. The cylinders were placed on their side to provide a 5 mm contact line perpendicular to the sliding direction. The tests were performed at temperature 300 °C, in a unidirectional rotational mode at 30 rpm, wear track radius 9 mm, 1.4 cm/s linear speed and an applied load of 20 N, which equals 0.24 GPa linear applied pressure. Raman spectra were collected during the tribology tests from the wear track region. To maximize the signal-to-noise ratio, each Raman spectrum was averaged over approximately 100 rotational cycles of the tribology tests.

Additional tribological tests were performed using an Anton Paar pin-on-disk TRB^3 tribometer, to determine the effects of temperature on friction and wear characteristics of the coatings. The uncoated aluminum sample (Al0) and the coated sample Al3 were tested against silicon nitride balls (6 mm in diameter) at temperatures from 25 °C to 300 °C (for sample details, see Table 1.) The tests were performed in a reciprocating mode with a 1.4 mm arc stroke length and 20° angle sliding at 1.4 cm/s maximum linear speed and 2 Hz frequency. The applied load and corresponding maximum contact pressure were in the range of 2–10 N and 0.83–1.43 GPa, respectively. Each test was repeated three times to confirm result reproducibility.

2.3. Characterization

Chemical analysis, elemental mapping and cross-sectional microscopy were conducted using FEI Quanta 200 SEM equipped with energy-dispersive X-ray spectroscopy (EDS). A focused ion beam (FIB) attachment to the FEI Quanta SEL was used for cross-section and TEM samples preparation. High-magnification micrographs were captured with TEM (FEI Tecnai G2 F20) using a 200 kV electron beam. Analysis of the wear tracks was performed using a Zeiss optical microscope. The composition of the coatings and corresponding phases were tested using the Rigaku Ultima III X-ray diffractometer (XRD) with Cu Kα X-ray source operated in θ-2θ scanning mode with 1°/min scanning rate and 0.02° step increments. Additionally, wear track chemical analysis of the samples was performed using X-ray photoelectron spectroscopy (XPS) with a high flux X-ray source with Aluminum anode for X-ray generation and quartz crystal monochromator to focus and scan the beam on the sample with the PHI Versaprobe apparatus on the samples cleaned before the analysis by 10 s of sputtering. Coating roughness analysis was performed using Veeco Dektak 150 stylus profilometer with 2.5 μm tip radius. The thermal conductivity of samples before and after coating deposition was analyzed by Thermal Conductivity Analyzer TPS 2500S using a hot-disk measurement setup. Thermal conductivity values for each of the samples are included in Table 1.

3. Results and discussion

The PEO-Chameleon coating schematic is shown in Fig. 1a. PEO-Chameleon coating shows up to 5 times reduction in thermal conductivity as compared to the bulk Al alloy (reduction from 158 to 33–40 W/mK, Table 1). This lower conductivity is due to intrinsically low thermal conductivity of Al-Si-O coatings, as linked to granular crystalline oxides, amorphous phases, and voids in the outer coating layers [39]. The cross-sectional and surface morphology micrographs of a typical PEO layer before application of chameleon top layer (Fig. 1b and c) revealed that the PEO coating surface features a coarse porous morphology which results in relatively high surface roughness (~35 μm Ra). After burnishing with the chameleon powder, the surface became smoother due to filling in some of the open pores, although large fluctuations in the surface roughness remained in the case of as-deposited PEO coating (Table 1). The elemental 2D maps of constituents (Fig. S1) confirm the presence of Sb, O, Mo, S, and C, and indicate the uniform distribution of the burnishing Sb_2O_3, MoS_2 and graphite components on the surface. The presence of Sb and O elements confirmed the formation of the Sb_2O_3; Mo and S indicate MoS_2; and C points out the graphite component of the coating.

The roughness of these materials after chameleon coating burnishing and the corresponding surface morphology are shown in Fig. 1d–f. The largest roughness values were recorded for Al1 (with Ra equal to 38.5 μm). Sample Al2 had smoother surfaces and did not show any cracks or delamination (Fig. 1f).

Fig. 2a and b display an XPS spectrum and an XRD pattern for sample Al2, respectively. The figures highlight the observed phases of Al_2O_3 from the PEO coating and all three burnished solid lubricant phases. Specifically, as indicated in the XPS analysis (Fig. 2a), the surface of the sample is composed of carbon (attributed to the graphite presence), Mo and S (attributed to the MoS_2), Sb (attributed to antimony oxide), Al (attributed to aluminum oxide) and oxygen. XRD analysis (Fig. 2b) confirms the coating phases' structure consistent with, γ-Al_2O_3 (cubic), α-Sb_2O_3 (cubic), MoS_2 (hexagonal), and graphite. This analysis confirms that the burnishing process retains highly ordered MoS_2, high (002) reflection intensity, as well as the cubic Sb_2O_3 and graphite structures from the powder precursors.

To monitor the chemical and structural evolution of the PEO-Chameleon coatings in the wear track surfaces of high-temperature sliding tests, the in-situ Raman tribometer setup shown schematically in Fig. 3a was used. The coefficient of friction (COF) values measured at 300 °C as a function of sliding cycles are provided in Fig. 3b. Sample Al2 exhibited lower and more stable COF with the value in the 0.18 range; higher COF value was measured for sample Al1 under the same test conditions. As shown in Table 1 and Fig. 1d, sample A12 displayed better uniformity and fewer surface defects, such as microcracks and coating delamination, due to lower surface roughness (Ra equals to 19.1 μm) compared to the other three samples. These results indicated that the frictional behavior of the coatings is very dependent on initial surface topography since the underlying rougher PEO layer can lead to more abrasion particle accumulation by breaking the Al-Si-O layer asperities during run-in events.

The coating surface tribo-chemical evolutions that occur as a result of tribological tests at 300 °C were analyzed by collecting Raman spectra from wear tracks at different test cycle intervals. Fig. 3c and d show Raman spectra for Al1 and Al2, respectively. Each spectrum represents data collected over 100 cycles of tribological testing. The presence of MoS_2 and Sb_2O_3phases was detected. Interestingly, the low intensity of the Raman peaks from graphite (at ~1560 cm^{-1}, Fig. S2) suggests that upon heating, the surface of the sample became deficient in graphite, possibly due to the oxidation of carbon.

An important observation was that none of the samples indicated the oxidation of the MoS_2 compound over the duration of the whole test. This is significant especially given that the chemical stability of MoS_2 is of prime importance to maintain a low COF over large sliding distances. The hexagonal MoS_2 peaks at 380 and 410 cm^{-1} [48] remain strong, with no indication of any peak shifts or any oxide formation during the tribotests at 300 °C (Fig. 3c and d).

Another important parameter is the relative concentration of the Sb_2O_3 to MoS_2 components, detected by the maximum peak ratio. Although the composition of the chameleon powder was the same for

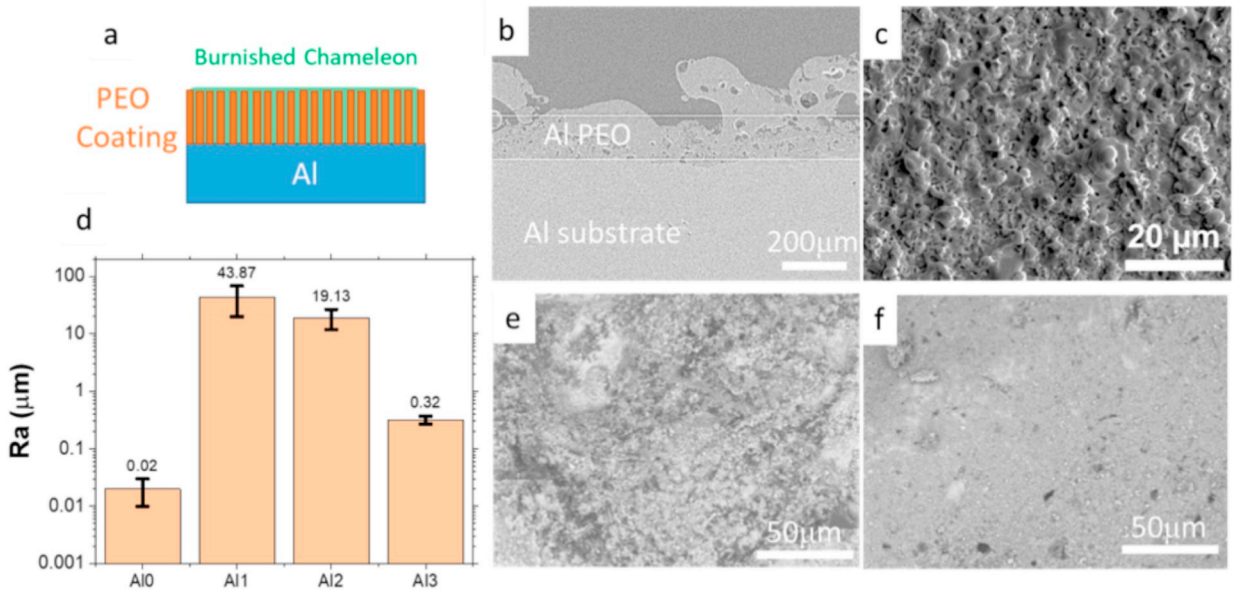

Fig. 1. (a) Schematic of Al PEO-Chameleon coatings tested in this study. (b) Cross-section of Al1 PEO before burnishing, (c) surface morphology of Al PEO before burnishing, (d) roughness of different coatings after burnishing. Surface morphology of Al1 (e) and Al2 (f) after burnishing.

the samples Al1 and Al2, the wear track surfaces demonstrate different relative compositions in the wear tracks (Fig. 3e). For sample Al1, which has a higher COF (Fig. 3b), this ratio is high (Fig. 3c). Meanwhile, for the sample Al2 with a lower COF, this ratio is also smaller (Fig. 3e). A similar trend is observed for the second batch of samples processed under similar conditions (Fig. S2). Therefore, the Sb_2O_3 to MoS_2 peak ratio would be another key factor affecting the lubrication properties during high-temperature tribology tests.

Changes in the Raman spectra during tribological testing indicate that Sb_2O_3 migrated to the bottom of the wear track, which is demonstrated by the intensity ratio of Sb_2O_3 to MoS_2 peaks (Fig. 3e) and is in agreement with earlier work [45]. Therefore, the improvement in tribological behavior is attributed to the enrichment of the surface with an active MoS_2 layer that facilitates sliding through the shearing mechanism.

Changes in the wear tracks were further analyzed by comparing EDS maps of Al1 and Al2 coatings after the tests. A yellow dashed line in Fig. 4 discerns areas inside and outside the wear track for the sample Al1 which demonstrated the higher COF. Although the coating outside the wear track was intact, inside it the chameleon layer (C, Mo, Sb maps) had almost completely vanished. EDS elemental maps of the wear tracks indicated the presence of Al, O, and Fe, which suggests that the chameleon coating was worn out during sliding, thus exposing the PEO sublayer to the contact with steel counterface. A presence of Fe (Fig. 4h) inside the wear track, as it is confirmed by high contrast in the Fe intensity, indicated mass transfer from the steel pin.

In contrast to Al1 (Fig. 4), EDS maps of the wear track in sample A12 clearly showed strong signals from all components of the chameleon layer, thereby confirming that its smooth surface was the main factor responsible for such behavior (Fig. 5). Strong and uniformly distributed intensities of Sb, O, Mo, S, and C inside the contact area at 300 °C support the conclusion that the chameleon coating remained effective over the duration of the test. The effectiveness of the chameleon coating resulted in low COF for the entire duration of the test.

To understand the fundamental mechanisms that facilitate the lubricious behavior of this complex duplex coating during sliding, EDS maps of the contact area of the cylinder counter body were collected (Fig. 6). The elemental maps indicated signs of mass transfer from the lubricous chameleon surface, hence providing lower shear stresses during sliding [45]. The presence of the transfer films is demonstrated

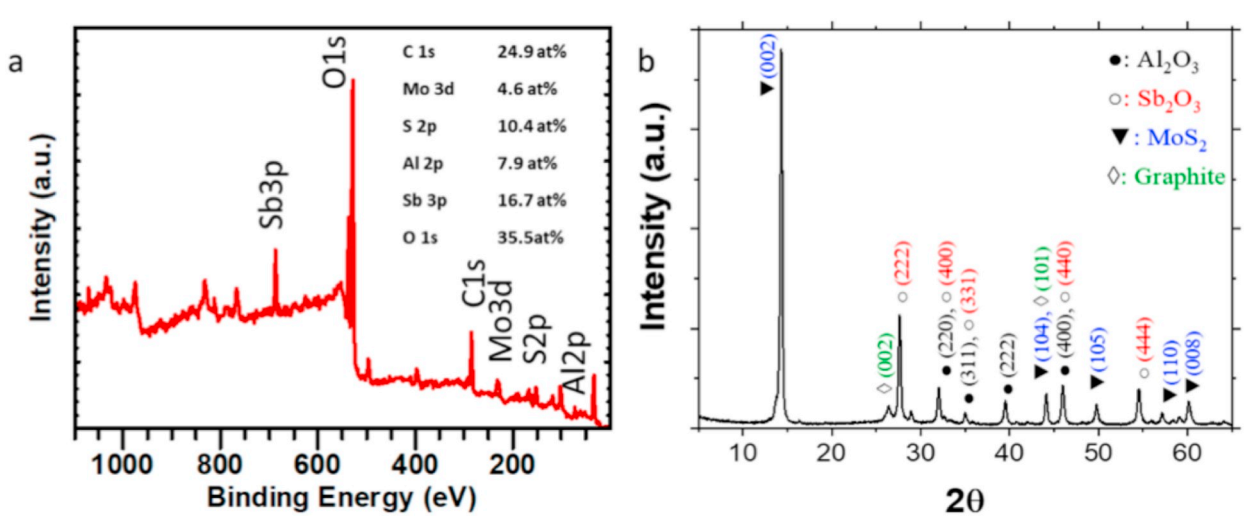

Fig. 2. (a) XPS of Al2 presenting C, Mo, S, Al, Sb and O elements. (b) XRD patterns of Al2 sample which shows Al_2O_3, Sb_2O_3, and MoS_2, and graphite peaks.

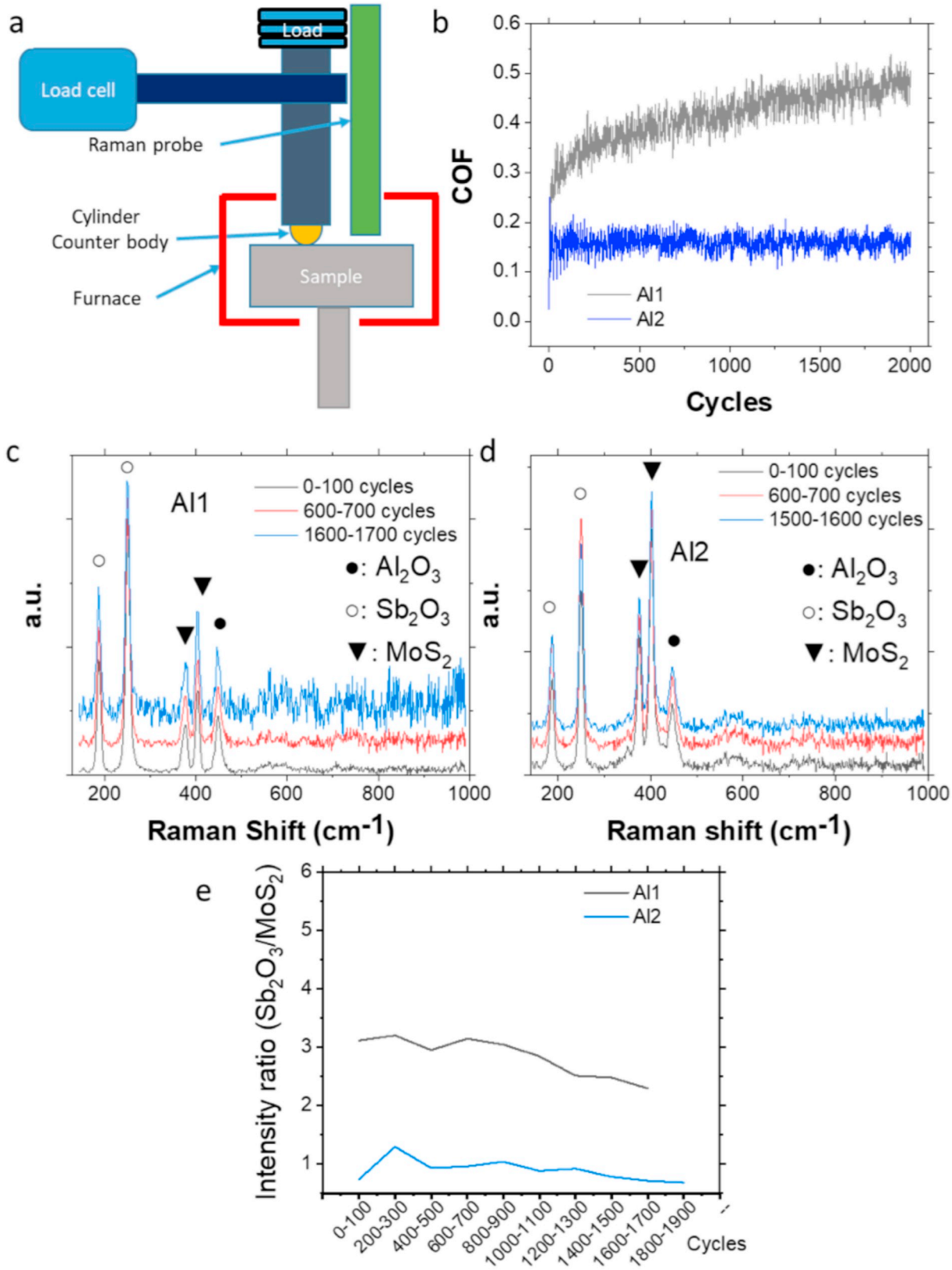

Fig. 3. (a) Schematic diagram of the in-situ Raman-Tribometer rig. (b) Frictional behavior of the studied samples at 300 °C. Recorded in-situ Raman spectra from wear track surfaces during sliding tests at 300 °C for (c) Al1 and (d) Al2 respectively. (e) Intensity ratio of Sb_2O_3 to MoS_2 as a function of sliding cycles.

by maps of Sb, O, Mo, and S on the steel counterface, signifying the mass transfer of both Sb_2O_3 and MoS_2. These two phases impart low frictional behavior due to the low-shearing nature of the materials [45]. Also, two important observations were inferred from the in-situ Raman studies of the PEO-Chameleon coatings: (i) the chameleon top layer effectively resists tribo-oxidation at 300 °C when residing on the hard wear-resistant PEO surface; and, (ii) low roughness values of the PEO layer are critical to retaining the chameleon layer. Once the chameleon

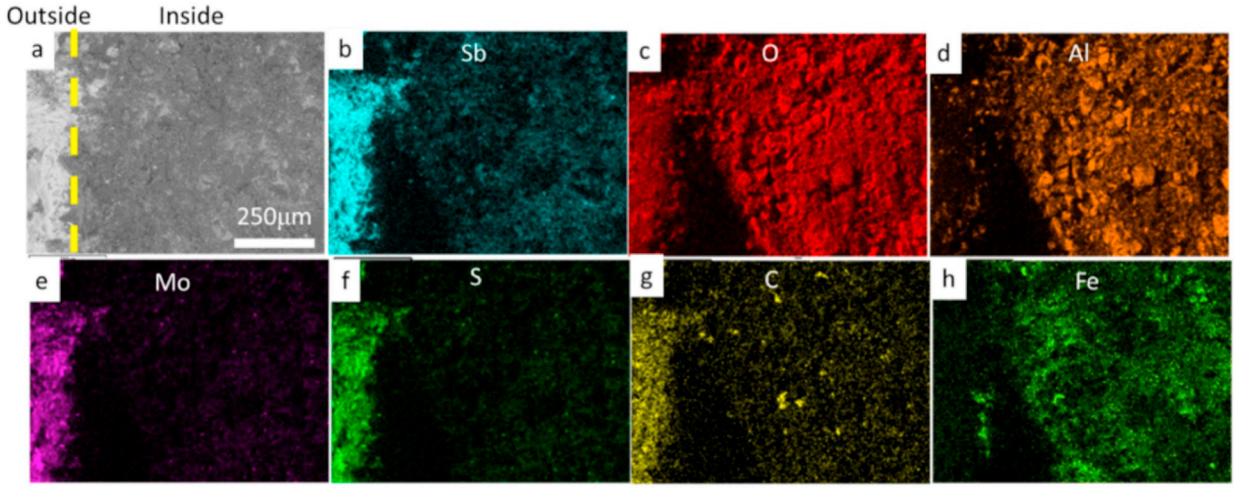

Fig. 4. (a) SEM micrograph of Al1 showing the boundary of wear track; dashed yellow line separates inside and outside the wear track. (b)–(g) show the EDS maps of (a) for Sb (b), O (c), Al (d), Mo (e), S (f), C (g) and Fe (h), respectively. (For interpretation of the references to colour in this figure legend, the reader is referred to the web version of this article.)

layer is consumed, the coating COF and endurance on keeping low friction behavior deteriorate.

Load and temperature influence on the behavior of the PEO-Chameleon coating.

The results reported above suggest that the roughness and the scale of open porosity of the PEO layer are the key parameters to achieving optimum frictional behavior of the duplex PEO-Chameleon coating. To analyze this hypothesis, the PEO coating was further polished to achieve a significantly lower surface roughness Ra = 3.4 µm, with finer open porosity, at the residual thickness of 28–32 µm (sample Al3, Table 1). The surface was subsequently burnished with the same chameleon powder that was described in the previous section to form a PEO-Chameleon coating. Fig. 7a shows the surface morphology of sample Al3 after burnishing. Its roughness before and after burnishing is reported in Fig. 7b and c. The final roughness is considerably lower than for the as-deposited and slightly polished samples (Al1 and A12).

Tribological testing of sample A13 was performed at both room and incrementally increased temperatures in sliding tests against a 6 mm diameter silicon nitride ball and at applied loads of 2, 5 and 10 N. These loads provided initial maximum Hertzian contact pressures of 0.83, 1.13, and 1.43 GPa, correspondingly. The results were compared to the data collected for a bare aluminum alloy sample without any surface treatment/modification (sample Al0 in Table 1). As expected, the COF values for Al3 were much lower than for the bare sample and varied in the 0.08–0.02 range depending on load and temperature. Room temperature tests conducted on the Al3 samples were performed with a normal load increased from 2 to 10 N. The results in Fig. 8a indicate reductions in friction from 0.2 to about 0.08 with an increase in the applied load. Noticeably, at a high applied load regime (10 N) the COF drops below 0.08, which is within the range of most high-performance lubricants [49]. In contrast, the bare Al0 sample did not exhibit any load dependence (Fig. 8b). Note, the COF for bare Al0 is significantly higher than that for Al3. Even larger COF values were previously reported for the PEO coating alone [33], which further emphasizes the importance of Chameleon composition for the improvements in tribological behavior of the duplex coating. Optical micrographs of contact areas revealed an order of magnitude difference between the wear track widths for the Al3 and Al0 samples (Fig. 8i). The bare Al0 samples show scuffing in all testing regimes (Fig. 8f–h), whereas Al3 samples displayed a very uniform wear track with no increase in its apparent width with the load increase; i.e., Al3 at 5 N and 10 N show similar wear track widths of 119.4 µm and 112.5 µm, respectively (Fig. 8d and e). This is

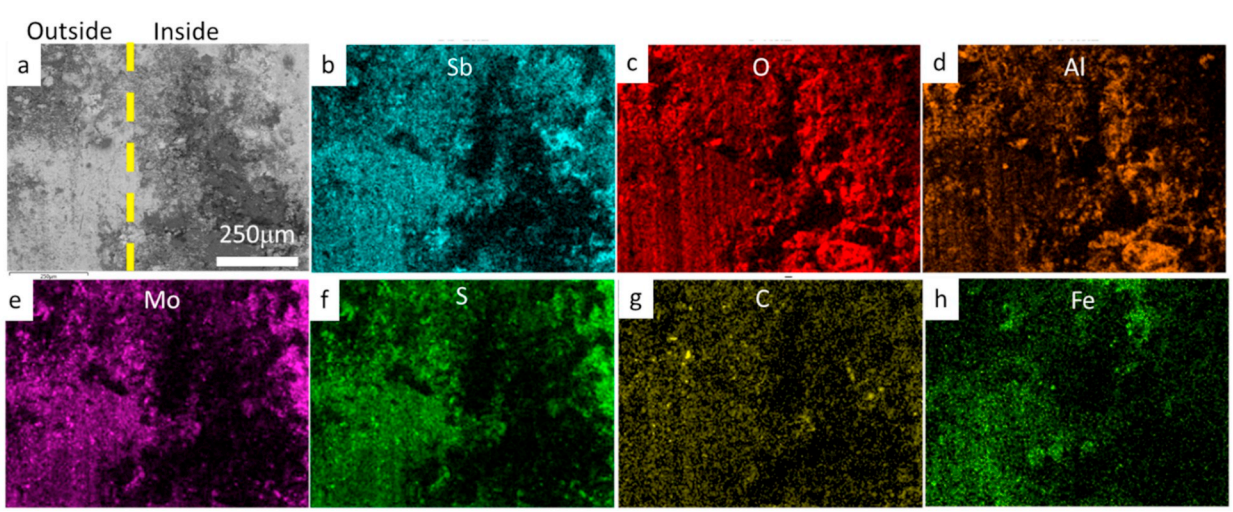

Fig. 5. (a) Represents SEM micrograph of Al2; dashed yellow line indicates the interface of wear track by intact outside area. EDS mapping images are shown for Sb (b), O (c), Al (d), Mo (e), S (f), C (g) and Fe (h), respectively. (For interpretation of the references to colour in this figure legend, the reader is referred to the web version of this article.)

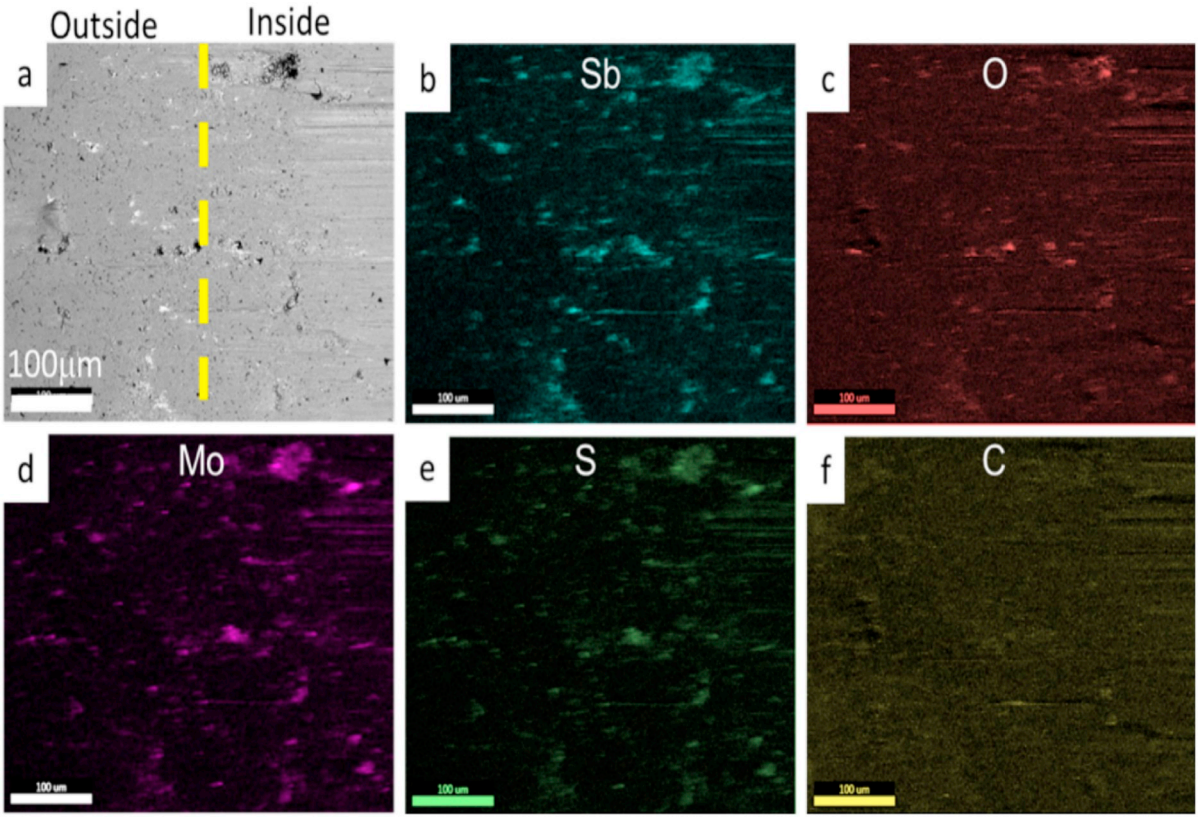

Fig. 6. (a) SEM micrograph of the counter body (cylinder) for the test against Al2, which shows the boundary of wear track by the dashed yellow line. Mass transfer on to the counter body is obvious as EDS mapping reveals Sb (b), O (c), Mo (d), S (e) and C (f), respectively. (For interpretation of the references to colour in this figure legend, the reader is referred to the web version of this article.)

attributed to the fact that higher loads induce more strain and localized friction heat, resulting in reorientation of basal planes along the wear tracks, which in turn lowers friction and wear of the coatings [45]. The observed variations in the COF behavior for Al3 sample indicate the coating transfer to and from the counter body, which is usually observed for easy shearing solid lubricants [50,51] and confirmed in the EDS analysis in Fig. 6.

Sliding tests with incrementally higher temperatures (25, 100, 200, 300 °C) were conducted for A13 and bare Al0 samples (Fig. 9). For the PEO-Chameleon coatings, the temperature increase from 25 to 300 °C further promoted the COF to decrease from 0.08 to 0.02 (Fig. 9b). The optical micrographs revealed that wear track width was 159.9 µm at 100 °C. However, at 300 °C, the wear track displayed a slight width reduction to 133.9 µm. Also, the effective contact area of the counter body exhibited the same reduction behavior from 234.5 µm at 100 °C to 158.4 µm at 300 °C.

In contrast to the PEO-Chameleon coating behavior, the increased temperature had a significant deteriorating effect on the frictional

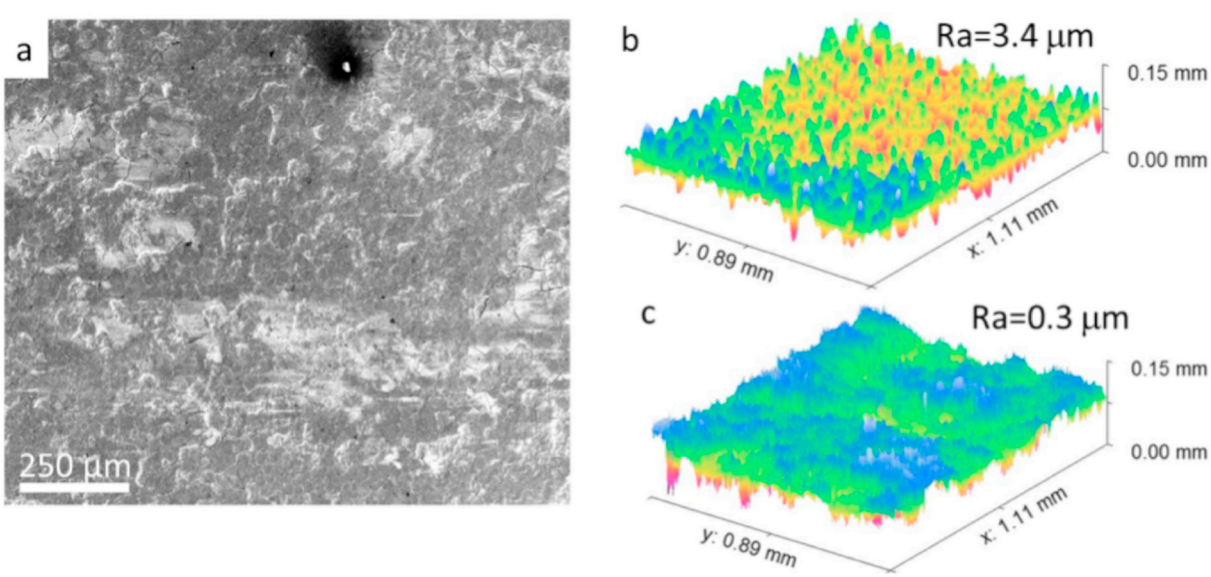

Fig. 7. (a) SEM micrograph of the Al3 sample. Surface roughness of the sample before (b) and after burnishing (c).

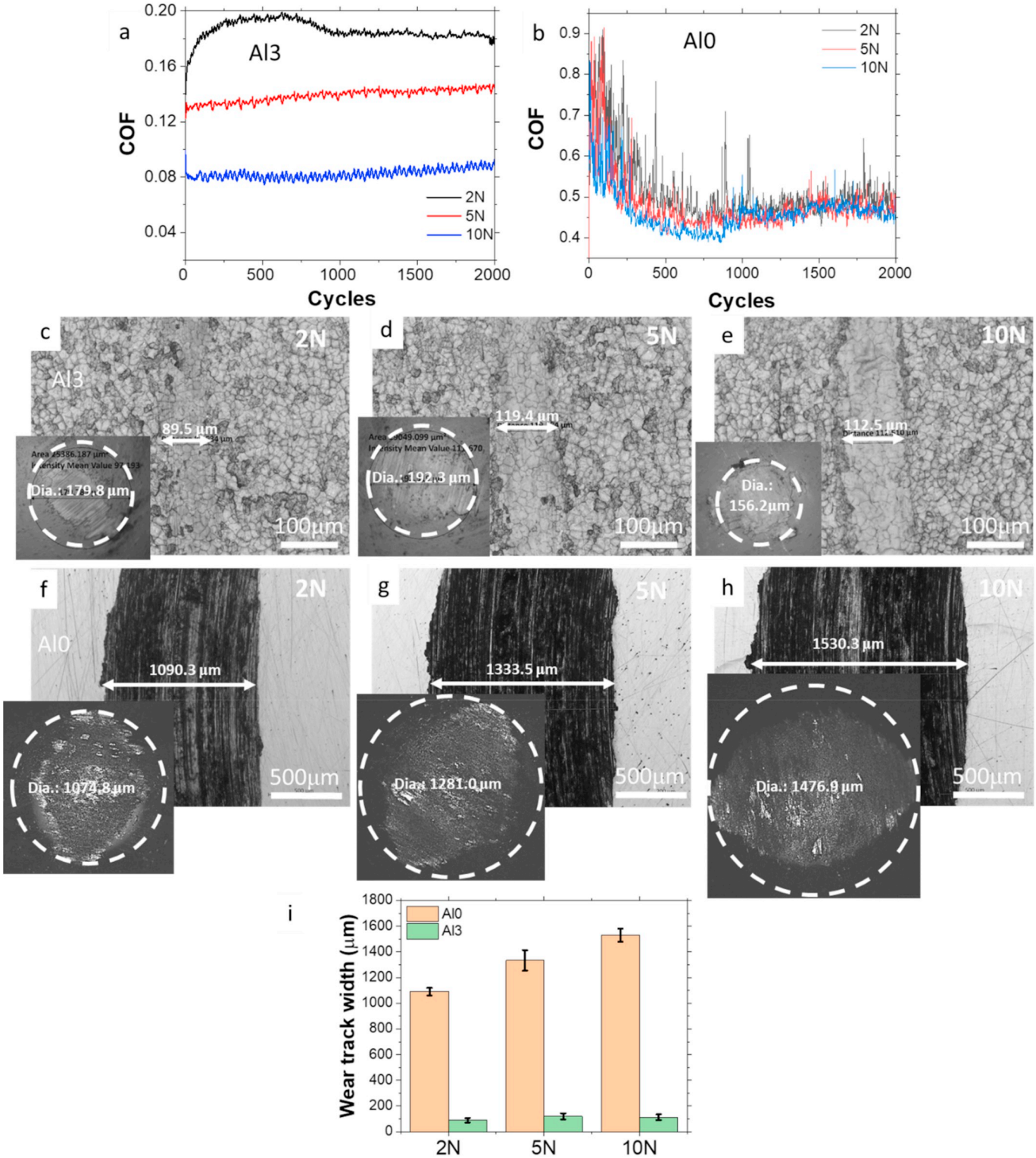

Fig. 8. Room temperature sliding test results: (a) Coefficient of friction as a function of load for PEO-Chameleon coating Al3; (b) coefficient of friction for a bare alloy as the reference; (c–e) optical micrographs of wear track and counterpart ball contact area for PEO-Chameleon Al3 coating after the tests at 2, 5 and 10 N correspondingly; (f–h) optical micrographs of wear track and counterpart ball contact area for bare Al0 sample after the tests at 2, 5 and 10 N correspondingly. (i) Comparative wear track width analysis for the samples Al0 and Al3.

behavior of the bare sample (Fig. 9a). Above 200 °C, aluminum started to develop scuffing behavior, which led to the formation of a large amount of debris and material transformation from the substrate to the Si_3N_4 counter body (Fig. S3). The Al0 sample displayed an order of magnitude larger wear track width; i.e., at 300 °C, the wear track of Al0 is 2025 µm (Fig. 9c).

A closer look inside and outside the wear track for sample A13 indicated a surface adaptive response, which may additionally contribute to high lubricity at 300 °C. Fig. 9d and e suggest that the area outside of the wear tracks was covered by micro-cracks spreading all across the

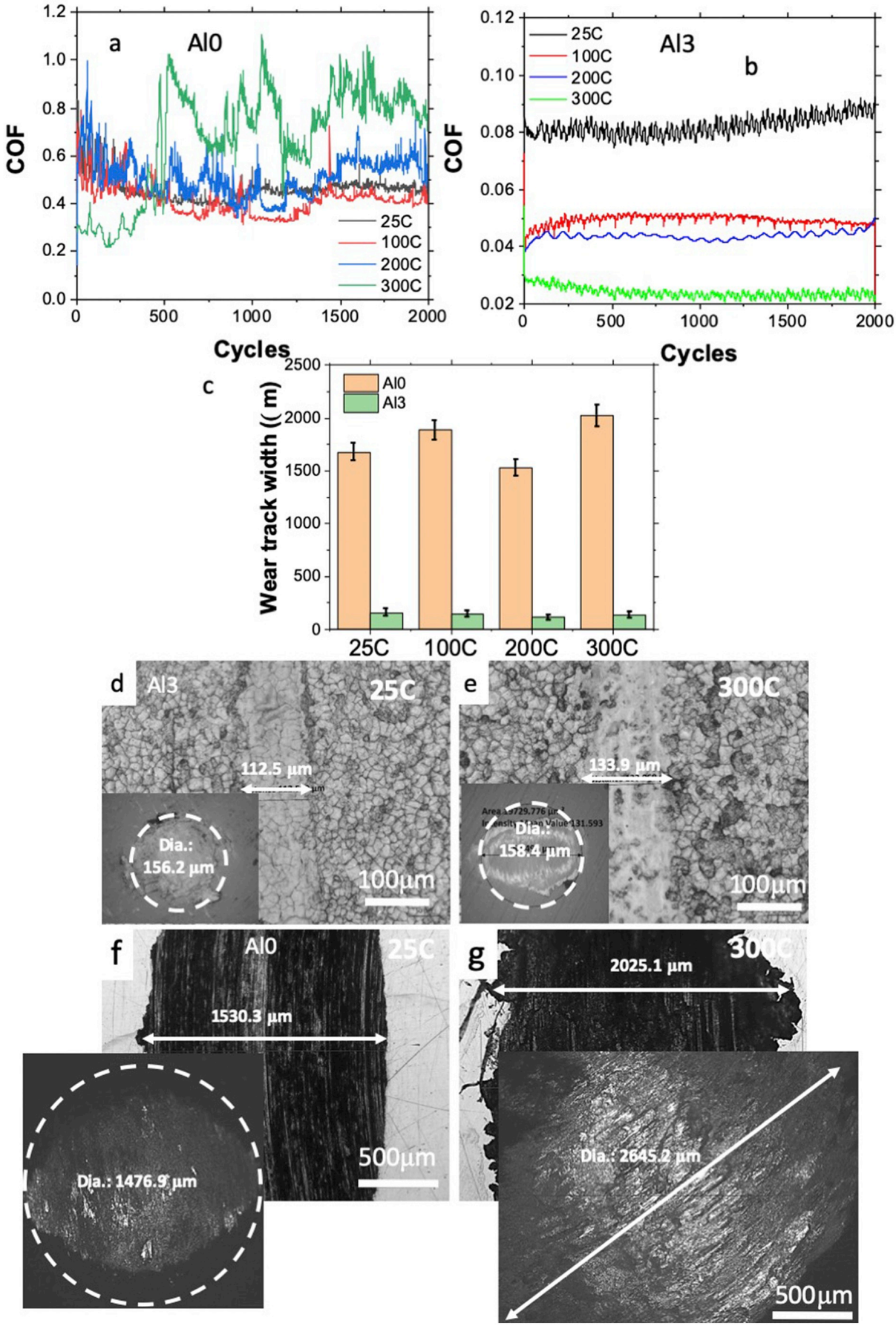

Fig. 9. COF values measured at different temperatures for Al0 (a) and Al3 (b) samples. Optical micrographs of contact area at 10 N and 25 °C (d & f) and 300 °C (e & g) for Al3 and Al0, respectively.

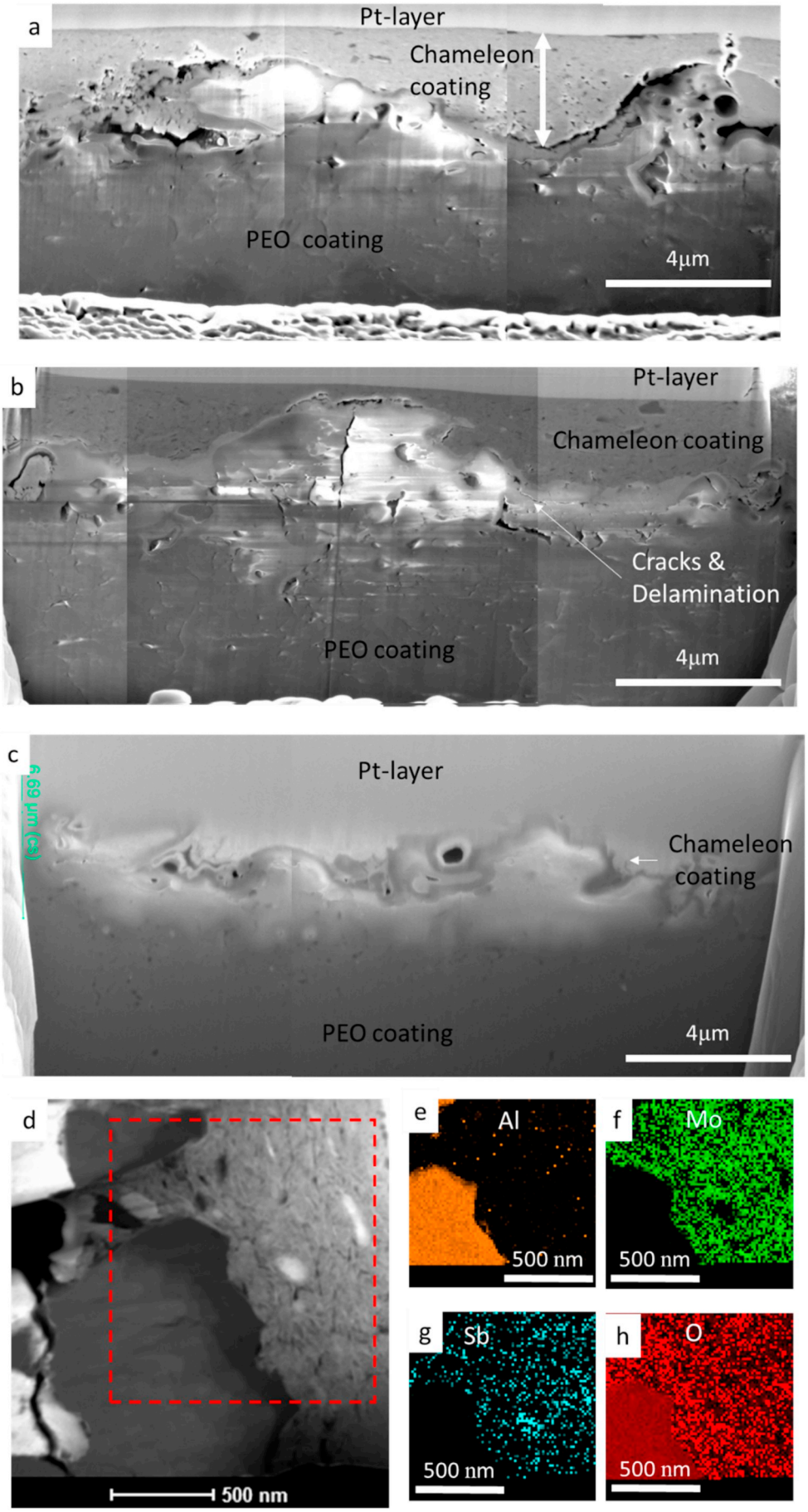

(caption on next page)

Fig. 10. Cross-sectional SEM micrograph of the coating outside the contact area (a) and inside the wear track for tests done at 25 °C (b) and 300 °C (c). TEM of the coating shows a higher magnification of interface between PEO coating and Chameleon-burnished phases inside the wear track (d). Elemental mapping of a selected area in (d) outlined by the dashed red line, Al (e), Mo (f), Sb (g), and O (h), respectively. (For interpretation of the references to colour in this figure legend, the reader is referred to the web version of this article.)

chameleon coating. However, inside the wear track, the surface appeared to be denser and displayed less surface cracking. Further analysis of wear tracks is included in Fig. S4. At temperatures < 100 °C, the cracks were still observed inside the track. But at temperatures above 200 °C, the wear tracks were denser and did not show any evidence of cracking.

To understand the underlying mechanism of crack propagation hindering and the superior lubricous behavior of the PEO-Chameleon coatings at elevated temperatures, FIB-assisted cross-sections were prepared for samples tested at 25 °C and 300 °C, in the regions inside and outside the contact areas (Fig. 10). The cross-sectional images reveal microcracks and unfilled pores outside of the wear track area (Fig. 10a). These become less apparent inside the wear track, while they are still detectable in cross-sectional images after tribotests at 25 °C (Fig. 10b). A plausible explanation is that repeated contact pressure and straining applied during sliding cause the phases forming the chameleon coating to be pushed farther inside the pores. This process is further enhanced as temperature increases to 300 °C, which leads to a better synergy at the interface between the PEO and the chameleon coating (Fig. 10c). High-resolution TEM micrographs and elemental maps of the sample A13 after the tests at 300 °C indicate that the initial porous structure of the PEO coating was completely filled with the chameleon powders and the microcracks of the lubricous chameleon phase were eliminated (Fig. 10d–h).

The above results indicate that temperature had a dominant effect on the frictional behavior of the duplex coatings investigated in this study. Specifically, the burnished phases covered microcracks and filled micropores, thus providing total interlocking of the top lubricating chameleon layer to the underlying load support and wear-resistant PEO coating. In addition, a temperature increase (up to 300 °C in this study) significantly improved the overall coating wear resistance and reduced the COF. Leading mechanisms for enhanced tribological properties were linked not only to the basal plane reorientation of adaptive chameleon coating behavior as reported earlier but also to a synergism between PEO and chameleon layers in response to increases in both temperature and load. The open morphology of hard PEO-produced Al-Si-O layer promotes the stability of the chameleon compositions while protecting it from the oxidation. As a result, the further cracking and material failure was prevented. The result was a well-anchored and well-adhered lubricious surface capable of acting as a reservoir of solid lubricant during sliding wear.

4. Conclusions

In this study, PEO-Chameleon coatings were produced on an aluminum alloy (A365) substrate. A porous morphology, especially in the surface region of the PEO layer, was found to be practically responsible for reduced thermal conductivity and contributes to the changes in surface roughness upon polishing. The application of the chameleon top layer reduced surface roughness significantly by filling in surface valleys and voids with the MoS_2-graphite-Sb_2O_3 powder. The residual surface roughness and porosity of the PEO layer have shown to be the key factor determining the tribological behavior of duplex PEO-Chameleon coatings, with a decrease by an order of magnitude in the COF (0.02 vs 0.2) when sliding against steel achieved by a reduction in the coating surface roughness, R_a, from 34 to 3 μm.

The PEO-Chameleon coating exhibited very stable behavior under the Hertzian maximum contact pressures increasing from 0.83 to 1.43 GPa; the wear track width displayed over an order of magnitude reduction (from 2025 μm to 134 μm) compared to the base Al alloy for the test conducted under combined high load and temperature (10 N, 300 °C). Such dramatic wear reduction was deemed to be due to the hard PEO layer supporting the solid lubricating layer which exhibited mass transfer of the lubricious chameleon phases (MoS_2 and graphite) onto the counter body followed by the formation of a low-shear transfer film under the applied thermo-mechanical stimuli.

The duplex PEO-Chameleon coating exhibited high thermo-mechanical stability. No degradation by oxidation of MoS_2 or graphite phase occurred with either sliding cycles or temperature increase. At the same time, consistent with previous reports, the Sb_2O_3 phase tended to accumulate below the surface, at the interface with the underlying PEO layer. Importantly, the increase in test temperature from room to 300 °C forced the material of the chameleon layer to fill the PEO layer porosity and cracks to provide easier sliding of the films. Thus, not only did this promote the healing of cracks and defects and improve the PEO-Chameleon coating resistance to fracture and fatigue in high-pressure contacts, but it also helped to protect MoS_2 and graphite lubricating phases from oxidation, thereby reducing the friction coefficient by an order of magnitude.

CRediT authorship contribution statement

Asghar Shirani:Investigation, Data curation, Writing - original draft, Writing - review & editing.**Tasha Joy**:Data curation.**Aleksey Rogov**:Resources.**Mengyu Lin**:Resources.**Aleksey Yerokhin**: Resources, Writing - original draft, Writing - review & editing.**Jon-Erik Mogonye**:Writing - original draft, Writing - review & editing.**Andras Korenyi-Both**:Resources.**Samir M. Aouadi**:Writing - original draft, Writing - review & editing.**Andrey A. Voevodin**:Supervision, Conceptualization, Writing - original draft, Writing - review & editing.**Diana Berman**:Supervision, Investigation, Conceptualization, Writing - original draft, Writing - review & editing.

Declaration of competing interest

The authors declare that they have no known competing financial interests or personal relationships that could have appeared to influence the work reported in this paper.

Acknowledgments

Parts of this research were supported by the U.S. CCDC Army Research Laboratory (Award No. W911NF-19-2-0281) and the European Research Council under the ERC Advanced Grant (320879 'IMPUNEP') and ERC-2018-PoC programme (825122 - 3D Cer-Met). This work was performed in part at the University of North Texas' Materials Research Facility. Support from Advanced Materials and Manufacturing Processes Institute (AMMPI) at the University of North Texas is acknowledged. The authors acknowledge Dr. Alam Talukder for a help with cross sectional FIB and TEM images.

Appendix A. Supplementary data

Supplementary data to this article can be found online at https://doi.org/10.1016/j.surfcoat.2020.126016.

References

[1] Q. Mehran, M. Fazal, A. Bushroa, S. Rubaiee, A critical review on physical vapor

deposition coatings applied on different engine components, Crit. Rev. Solid State 43 (2018) 158–175.
[2] B. Gérard, Application of thermal spraying in the automobile industry, Surf. Coat. Technol. 201 (2006) 2028–2031.
[3] D. Choi, S. Lee, S. Kim, P. Lee, K. Lee, H. Park, W. Hwang, Dependence of adhesion and friction on porosity in porous anodic alumina films, Scr. Mater. 58 (2008) 870–873.
[4] H.-s. Kim, D.-h. Kim, W. Lee, S.J. Cho, J.-H. Hahn, H.-S. Ahn, Tribological properties of nanoporous anodic aluminum oxide film, Surf. Coat. Technol. 205 (2010) 1431–1437.
[5] T. Hu, L. Hu, The study of tribological properties of laser-textured surface of 2024 aluminium alloy under boundary lubrication, Lubr. Sci. 24 (2012) 84–93.
[6] R. Zhou, J. Cao, Q.J. Wang, F. Meng, K. Zimowski, Z.C. Xia, Effect of EDT surface texturing on tribological behavior of aluminum sheet, J. Mater. Process. Technol. 211 (2011) 1643–1649.
[7] G. Fox-Rabinovich, K. Yamomoto, S. Veldhuis, A. Kovalev, G. Dosbaeva, Tribological adaptability of TiAlCrN PVD coatings under high performance dry machining conditions, Surf. Coat. Technol. 200 (2005) 1804–1813.
[8] J. Batista, C. Godoy, G. Pintaúde, A. Sinatora, A. Matthews, An approach to elucidate the different response of PVD coatings in different tribological tests, Surf. Coat. Technol. 174 (2003) 891–898.
[9] S. Hogmark, S. Jacobson, M. Larsson, Design and evaluation of tribological coatings, Wear 246 (2000) 20–33.
[10] T. Romsdahl, A. Shirani, R.E. Minto, C. Zhang, E.B. Cahoon, K.D. Chapman, D. Berman, Nature-guided synthesis of advanced bio-lubricants, Sci. Rep. 9 (2019) 11711.
[11] A. Cameron, The Principles of Lubrication, Wiley, 1966.
[12] X. Li, A.M. Teitgen, A. Shirani, J. Ling, L. Busta, R.E. Cahoon, W. Zhang, Z. Li, K.D. Chapman, D. Berman, C. Zhang, R.E. Minto, E.B. Cahoon, Discontinuous fatty acid elongation yields hydroxylated seed oil with improved function, Nat. Plants 4 (2018) 711–720.
[13] W.J. Bartz, Engine Oils and Automotive Lubrication, Routledge, 2019.
[14] K. Jacques, T. Joy, A. Shirani, D. Berman, Effect of water incorporation on the lubrication characteristics of synthetic oils, Tribol. Lett. 67 (2019) 105.
[15] S.M. Aouadi, H. Gao, A. Martini, T.W. Scharf, C. Muratore, Lubricious oxide coatings for extreme temperature applications: a review, Surf. Coat. Technol. 257 (2014) 266–277.
[16] K. Holmberg, A. Matthews, Coatings Tribology: Properties, Mechanisms, Techniques and Applications in Surface Engineering, Elsevier, 2009.
[17] T. Polcar, A. Cavaleiro, High-temperature tribological properties of CrAlN, CrAlSiN and AlCrSiN coatings, Surf. Coat. Technol. 206 (2011) 1244–1251.
[18] F.P. Bowden, F.P. Bowden, D. Tabor, The Friction and Lubrication of Solids, Oxford University Press, 2001.
[19] D. Stone, J. Liu, D.P. Singh, C. Muratore, A.A. Voevodin, S. Mishra, C. Rebholz, Q. Ge, S.M. Aouadi, Layered atomic structures of double oxides for low shear strength at high temperatures, Scr. Mater. 62 (2010) 735–738.
[20] S.M. Aouadi, D.P. Singh, D. Stone, K. Polychronopoulou, F. Nahif, C. Rebholz, C. Muratore, A.A. Voevodin, Adaptive VN/Ag nanocomposite coatings with lubricious behavior from 25 to 1000 °C, Acta Mater. 58 (2010) 5326–5331.
[21] H. Gao, A. Otero-de-la-Roza, J. Gu, D.A. Stone, S.M. Aouadi, E.R. Johnson, A. Martini, (Ag, Cu)–Ta–O ternaries as high-temperature solid-lubricant coatings, ACS Appl. Mater. Interfaces 7 (2015) 15422–15429.
[22] A. Shirani, J. Gu, B. Wei, J. Lee, S.M. Aouadi, D. Berman, Tribologically enhanced self-healing of niobium oxide surfaces, Surf. Coat. Technol. 364 (2019) 273–278.
[23] C. Muratore, A.A. Voevodin, Chameleon coatings: adaptive surfaces to reduce friction and wear in extreme environments, Annu. Rev. Mater. Res. 39 (2009) 297–324.
[24] T. Scharf, S. Prasad, Solid lubricants: a review, J. Mater. Sci. 48 (2013) 511–531.
[25] J.F. Curry, N. Argibay, T. Babuska, B. Nation, A. Martini, N.C. Strandwitz, M.T. Dugger, B.A. Krick, Highly oriented MoS_2 coatings: tribology and environmental stability, Tribol. Lett. 64 (2016) 11.
[26] D. Berman, A. Erdemir, A.V. Sumant, Graphene: a new emerging lubricant, Mater. Today 17 (2014) 31–42.
[27] J. Eichler, C. Lesniak, Boron nitride (BN) and BN composites for high-temperature applications, J. Eur. Ceram. Soc. 28 (2008) 1105–1109.
[28] W. Bollmann, J. Spreadborough, Action of graphite as a lubricant, Nature 186 (1960) 29–30.
[29] D. Berman, K.C. Mutyala, S. Srinivasan, S.K.R.S. Sankaranarayanan, A. Erdemir, E.V. Shevchenko, A.V. Sumant, Iron-nanoparticle driven tribochemistry leading to superlubric sliding interfaces, Adv. Mater. Interfaces 6 (2019) 1901416.
[30] D. Berman, S.A. Deshmukh, S.K.R.S. Sankaranarayanan, A. Erdemir, A.V. Sumant, Macroscale superlubricity enabled by graphene nanoscroll formation, Science 348 (2015) 1118–1122.
[31] J.L. Li, D.S. Xiong, Tribological properties of nickel-based self-lubricating composite at elevated temperature and counterface material selection, Wear 265 (2008) 533–539.
[32] A. Voevodin, T. Fitz, J. Hu, J. Zabinski, Nanocomposite tribological coatings with “chameleon” surface adaptation, J. Vac. Sci. Technol. A 20 (2002) 1434–1444.
[33] Y.-F. Liu, T. Liskiewicz, A. Yerokhin, A. Korenyi-Both, J. Zabinski, M. Lin, A. Matthews, A.A. Voevodin, Fretting wear behavior of duplex PEO/chameleon coating on Al alloy, Surf. Coat. Technol. 352 (2018) 238–246.
[34] A. Yerokhin, X. Nie, A. Leyland, A. Matthews, S. Dowey, Plasma electrolysis for surface engineering, Surf. Coat. Technol. 122 (1999) 73–93.
[35] A. Voevodin, A. Yerokhin, V. Lyubimov, M. Donley, J. Zabinski, Characterization of wear protective Al-Si-O coatings formed on Al-based alloys by micro-arc discharge treatment, Surf. Coat. Technol. 86 (1996) 516–521.
[36] N. Barati, E. Meletis, F.G. Fard, A. Yerokhin, S. Rastegari, M. Faghihi-Sani, Al2O3–ZrO2 nanostructured coatings using DC plasma electrolytic oxidation to improve tribological properties of Al substrates, Appl. Surf. Sci. 356 (2015) 927–934.
[37] R. Khan, A. Yerokhin, T. Pilkington, A. Leyland, A. Matthews, Residual stresses in plasma electrolytic oxidation coatings on Al alloy produced by pulsed unipolar current, Surf. Coat. Technol. 200 (2005) 1580–1586.
[38] W. Xue, C. Wang, Y. Li, R. Chen, T. Zhang, Analyses of microarc oxidation coatings formed on Si-containing cast aluminum alloy in silicate solution, ISIJ Int. 42 (2002) 1273–1277.
[39] M. Zhu, Z. Cai, X. Lin, P. Ren, J. Tan, Z. Zhou, Fretting wear behaviour of ceramic coating prepared by micro-arc oxidation on Al–Si alloy, Wear 263 (2007) 472–480.
[40] G. Sabatini, L. Ceschini, C. Martini, J. Williams, I. Hutchings, Improving sliding and abrasive wear behaviour of cast A356 and wrought AA7075 aluminium alloys by plasma electrolytic oxidation, Mater. Des. 31 (2010) 816–828.
[41] K. Li, W. Li, G. Zhang, W. Zhu, F. Zheng, D. Zhang, M. Wang, Effects of Si phase refinement on the plasma electrolytic oxidation of eutectic Al-Si alloy, J. Alloys Compd. 790 (2019) 650–656.
[42] J. He, Q. Cai, H. Luo, L. Yu, B. Wei, Influence of silicon on growth process of plasma electrolytic oxidation coating on Al–Si alloy, J. Alloys Compd. 471 (2009) 395–399.
[43] I.J. Hwang, D.Y. Hwang, Y.M. Kim, B. Yoo, D.H. Shin, Formation of uniform passive oxide layers on high Si content Al alloy by plasma electrolytic oxidation, J. Alloys Compd. 504 (2010) S527–S530.
[44] H.-j. Xie, Y.-l. Cheng, S.-x. Li, J.-h. Cao, C. Li, Wear and corrosion resistant coatings on surface of cast A356 aluminum alloy by plasma electrolytic oxidation in moderately concentrated aluminate electrolytes, Trans. Nonferrous Metals Soc. China 27 (2017) 336–351.
[45] J. Zabinski, J. Bultman, J. Sanders, J. Hu, Multi-environmental lubrication performance and lubrication mechanism of $MoS_2/Sb_2O_3/C$ composite films, Tribol. Lett. 23 (2006) 155–163.
[46] C. Muratore, J.E. Bultman, S.M. Aouadi, A.A. Voevodin, In situ Raman spectroscopy for examination of high temperature tribological processes, Wear 270 (2011) 140–145.
[47] E. Parfenov, A. Yerokhin, A. Matthews, Impedance spectroscopy characterisation of PEO process and coatings on aluminium, Thin Solid Films 516 (2007) 428–432.
[48] H. Li, Q. Zhang, C.C.R. Yap, B.K. Tay, T.H.T. Edwin, A. Olivier, D. Baillargeat, From bulk to monolayer MoS2: evolution of Raman scattering, Adv. Funct. Mater. 22 (2012) 1385–1390.
[49] A. Erdemir, Solid lubricants and self-lubricating films, in: B. Bhushan (Ed.), Handbook of Modern Tribology, CRC Press, 2001, pp. 787–818.
[50] R. Cai, Z. Chen, X. Nie, Alumina-based coating with dimples as enabling sustainable technology to reduce wear and emission of the brake system, ACS Sustain. Chem. Eng. 8 (2019) 893–899.
[51] R. Cai, J. Zhang, X. Nie, J. Tjong, D.T.A. Matthews, Wear mechanism evolution on brake discs for reduced wear and particulate emissions, Wear (2020) 203283.